Electronic structure and magnetic properties of CePdSb and Ce$_{1-x}$La$_x$PdSb

A. Ślebarski and W. Głogowski

Institute of Physics, University of Silesia, 40-007 Katowice, Poland

A. Jezierski

Institute of Molecular Physics, Polish Academy of Sciences, 60-179 Poznań, Poland

J. Deniszczyk

Institute of Physics and Chemistry of Metals, University of Silesia, 40-007 Katowice, Poland

A. Czopnik and A. Zygmunt

Institute for Low Temperature and Structure Research, Polish Academy of Sciences, 50-950 Wrocław, Poland

Using the various full-potential linear augmented plane wave (LAPW) methods we have studied the band structure of CePdSb and Ce$_{1-x}$La$_x$PdSb series of compounds. In the band calculations, CePdSb is half-metallic, i.e., metallic for majority spin while semiconducting for minority spin bands. The spin-polarized linearized muffin-tin orbital method also shows a half-metallic behavior of the Ce$_{1-x}$La$_x$PdSb compounds. The magnetic investigations and the electrical resistivity data indicate the existence of a ferromagnetic state in Ce$_{1-x}$La$_x$PdSb for $x \lesssim 0.7$. The sample Ce$_{0.1}$La$_{0.9}$PdSb is nonmagnetic and shows the power-law exponents in its susceptibility $\Delta\chi$, resistivity $\Delta\rho$, and specific heat $\Delta C/T$ temperature dependences indicative of the non-Fermi liquid behavior. The $3d$ x-ray photoemission spectroscopy (XPS) spectra indicate the occupation number of the f-shell, $n_f = 1$, in CePdSb and Ce$_{1-x}$La$_x$PdSb compounds. Analysis of the $3d^9 f^2$ weight in the $3d$ XPS spectra using Gunnarsson–Schönhammer theory suggests the f-states and conduction electron-states hybridization interaction Δ of about 80 meV for different configurations x of the system. We interpret the XPS data in terms of the band-structure calculations.

I. INTRODUCTION

Band structure calculations carried out from first principles have led to the discovery of a class of itinerant magnetic intermetallic compounds, having an energy gap for the partial density of states (DOS) for one of the spin projections.[1] As a consequence there is complete spin polarization of the conduction electrons at the Fermi level. These compounds are metallic, e.g., for majority, but semiconducting for minority spin electrons. They have therefore been called *half-metallic ferromagnets* (HMFs). Standard examples of HMFs are the semi-Heusler alloys NiMnSb and PtMnSb.[1] The complete spin polarization of the charge carriers at low temperatures have important consequences for magnetic and electric transport properties:

(i) HMF easily achieves the maximum saturation magnetization because a further increase in the spin splitting in this state does not increase the magnetic moment.

(ii) The temperature dependence of the resistivity in the range $T < T_C$ is dominated by a two-magnon process which gives rise to different power exponents[2] in $\rho(T)$ than a one-magnon scattering process (spin-flip scattering) expected for conventional metallic ferromagnets, for which $\rho \propto I^2 N_\uparrow(\epsilon_F) N_\downarrow(\epsilon_F)(T/T_C)$,[2] where I is the d-s exchange parameter and $N_\sigma(\epsilon_F)$ is the spin polarized DOS at the Fermi level.[3]

Our band structure calculations show that a state very close to a HMF with near zero-density $N_\downarrow(\epsilon_F)$ also appears in CePdSb. CePdSb has been known as a ferromagnet with a

Kondo-lattice behavior.[4] An idea to put CePdSb into a group of half-metallic ferromagnets is new.

On the base of HMF ground state properties of CePdSb we discuss its magnetic properties and electrical resistivity $\rho(T)$ data. We also investigate the solid solutions Ce$_{1-x}$La$_x$PdSb to determine the influence of alloying on the nature of the ground state across the series, when trivalent magnetic Ce in CePdSb is replaced by nonmagnetic La.

We have performed spin-polarized LMTO band structure calculations on the Ce$_{1-x}$La$_x$PdSb series, which show also a half-metallic band, i.e., an energy gap at ε_F inside the spin subbands $N_\downarrow(E)$ for the components $x \gtrsim 0.1$. Therefore, the temperature dependences of ρ and χ obtained for the Ce$_{1-x}$La$_x$PdSb series are also discussed in terms of the half-metallic ground state properties.

The first part of the paper contains a discussion of the system Ce$_{1-x}$La$_x$PdSb by high-energy probe and is followed by its characterization in terms of an overall single-particle electronic structure. We compare the valence band (VB) XPS spectra with the electronic-structure calculations for the valence bands. In the second part we present new experimental data on resistivity and susceptibility of Ce$_{1-x}$La$_x$PdSb series. We discuss the temperature dependence of the resistivity and the susceptibility which could result from the half-metallic properties. We also report an unusual temperature dependence of $\chi(T)$, $\rho(T)$ and specific heat $C(T)$ divided by T, $C(T)/T$, for a Ce$_{0.1}$La$_{0.9}$PdSb sample.
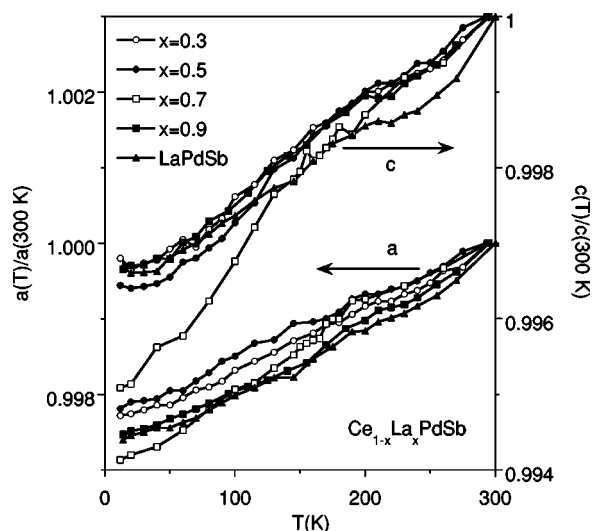
FIG. 1. The temperature dependence of $a(T)/a(300 \text{ K})$ and $c(T)/c(300 \text{ K})$ ratio for $Ce_{1-x}La_xPdSb$ polycrystalline samples.

II. EXPERIMENTAL DETAILS

Polycrystalline samples of $Ce_{1-x}La_xPdSb$ have been prepared by arc melting the constituent elements (Ce 99.99%, La 99.9%, Pd 99.999%, Sb 99.99% in purity) on a water cooled copper hearth in a high purity argon atmosphere with a Zr getter. Each sample was remelted several times to promote homogeneity and annealed at 800 °C for 2 weeks, and then quenched in water. The samples were carefully examined by x-ray diffraction analysis (Siemens D-5000 diffractometer) and found to consist of a single-phase. Analysis of the x-ray diffraction patterns with the Powder-Cell program revealed that the samples are hexagonal (space group $P6_3mc$). Shown in Fig. 1 is a comparison of the reduced lattice parameters $a(T)/a(300 \text{ K})$ and $c(T)/c(300 \text{ K})$ determined from x-ray-diffraction measurements at various temperatures T for the $Ce_{1-x}La_xPdSb$ series. The lattice thermal expansion obtained respectively in the a and c directions is almost the same for the different compounds of the $Ce_{1-x}La_xPdSb$ series, indicative of the comparable phonon contribution to the electrical resistivity of the investigated compounds.

The electrical resistivity was measured with the four-point method in the temperature region 4.2–300 K.

The dc magnetization was measured using a commercial SQUID magnetometer from 1.8 K to 400 K in magnetic fields up to of 5 T.

The XPS spectra were obtained with monochromatized Al K_α radiation at room temperature using a PHI 5700 ESCA spectrometer. The spectra were measured immediately after cleaving the sample in a vacuum of 10^{-10} Torr. A very small amount of oxygen could barely be detected in the noise of the XPS spectra. Calibration of the spectra was performed according to Ref. 5. Binding energies were referenced to the Fermi level ($\epsilon_F = 0$).

The electronic structure of $Ce_{1-x}La_xPdSb$ was studied by the self-consistent tight binding linearized muffin-tin orbital (LMTO) method[6] within the atomic sphere approximation (ASA) and the local spin density approximation (LSDA). The exchange correlation (XC) potential was assumed in the form proposed by von Barth–Hedin[7] and Langreth–Mehl–Hu (LMH) corrections were included.[8] The electronic structure was computed for the experimental lattice parameters for the supercell model. The values of the atomic Wigner–Seitz (W-S) sphere radii were chosen in such a way that the sum of all atomic sphere volumes was equal to the volume of the unit cell.

To test the reliability of the approximate TB LMTO results and to investigate the effect of the Coulomb correlation interaction within the Ce-$4f$ band states, the electronic structure of the stoichiometric CePdSb was also studied by the general potential (full potential) linear augmented plane wave (FP-LAPW) method. The calculations were performed using the the WIEN2K code.[9] In the FP-LAPW approach the crystal potential is expanded into spherical (lattice) harmonics within the muffin-tin (MT) atomic spheres and into plain waves outside MT spheres.

The FP-LAPW calculations were performed with the use of the gradient corrected LSD XC potential in the form developed by Perdew, Burke and Ernzerhof (PBE).[10] The electronic structure of CePdSb was studied by means of FP-LAPW with the use of the PBE XC potential, corrected according to the LSDA+U method[11] to account for the Hubbard correlation interaction within the $4f$-band states. The LSDA+U XC potential was implemented for the $4f$ orbitals of Ce atoms with the values of the Coulomb (U) and exchange (J) parameters equal to respectively 6.7 and 0.68 eV (Ref. 12). The calculations have been spin-polarized and all relativistic effects have been taken into account. The valence electrons were calculated within the scalar relativistic approach including spin-orbit interaction, using second variational method.

III. RESULTS AND DISCUSSION

A. Electronic structure of $Ce_{1-x}La_xPdSb$

X-ray photoemission spectroscopy is a powerful technique for studying the electronic properties of solids near the Fermi level. Such studies can be used to determine the density of states of the alloy, and, more interestingly, the contribution of the constituent elements to the valence bands. The XPS valence bands of $Ce_{1-x}La_xPdSb$ are compared in Fig. 2. The bands extend from Fermi energy located at $E=0$ to a binding energy of $\sim$12 eV. The VB XPS spectra are characterized by the major peaks located at $\sim$3.5 eV. A detailed comparison shows that a half width of the VB XPS peak roughly does not depend on the concentration of La (excluding a case of the $Ce_{0.5}La_{0.5}PdSb$ sample), and is about 3 eV. This suggests similar partial distributions of the Pd d states in the bands. The VB XPS spectra of $Ce_{1-x}La_xPdSb$ also show a weak hump around 10 eV binding energy that indicates the Sb s valence band states. In Fig. 2, we present numerical calculations of the electronic density of states of $Ce_{1-x}La_xPdSb$. Also shown in the figure, for comparison, are the XPS VB spectra. The spectra were measured at room temperature, i.e., much above the Curie temperature, therefore, to obtain a better agreement between the experimental
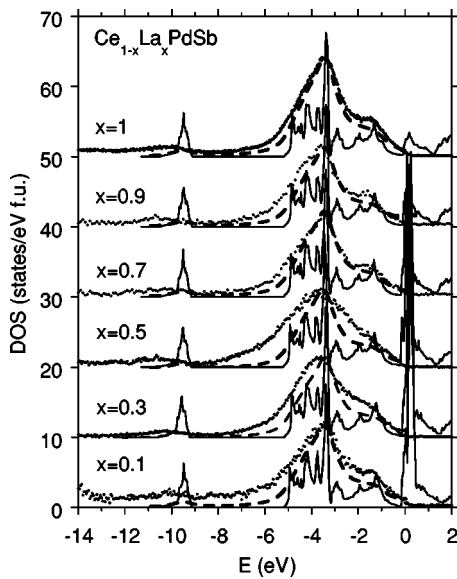
FIG. 2. The total DOS calculated for paramagnetic $Ce_{1-x}La_xPdSb$ (thin curve) convoluted by Lorentzians of half-width 0.4 eV, taking into account proper photoelectron cross sections for bands with different l symmetries (dashed line), compared to the measured XPS valence-band data corrected by background (points).

and calculated bands we compare in Fig. 2 the XPS valence band spectra with the calculated one for paramagnetic compounds. The densities of states were convoluted by Lorentzians with a half-width 0.4 eV to account for the instrumental resolution. The partial densities of states were multiplied by the corresponding cross sections.[13] A background, calculated by a Tougaard and Sigmund algorithm,[14] was subtracted from the XPS data. The experimental spectra are qualitatively very similar to the approximated DOS curve. We note very good agreement of the combined plots, especially in the low-energy region of the VB.

For the compounds of the series $Ce_{1-x}La_xPdSb$ the total DOS spectra decomposes into two clearly separated parts. A band located in the binding energy (BE) range of ~ 9–10.5 eV and separated by a gap of ~ 4 eV from the valence band originates mainly from the s states of Sb. The part of the valence-band which extends from 5 eV to ϵ_F is composed mainly of Pd $4d$ states. The Ce $4f$ states become dominant of the total DOS around the Fermi level. In the calculated densities of states we obtained the pseudogap located in the bands near the Fermi energy, having almost 0 DOS value (Fig. 3). The substitution of Ce by La decreases the number of f electrons, in result the pseudogap continuously moves towards the Fermi level (see Fig. 3). However, a standard resolution of only 0.4 eV of the measured VB XPS spectra makes discussion of this pseudogap enegetic shift impossible, even though the recorded spectra are qualitatively similar to the approximated DOS curves.

The majority and minority [which we will refer to as up ($\uparrow$) and down ($\downarrow$)] band structure resulting from various FP-LAPW methods (LDA, LDA+SO, LDA+SO+U) are shown in Fig. 4.

(i) The shape of the DOS generally does not depend on the method used for the calculations, excluding the narrow
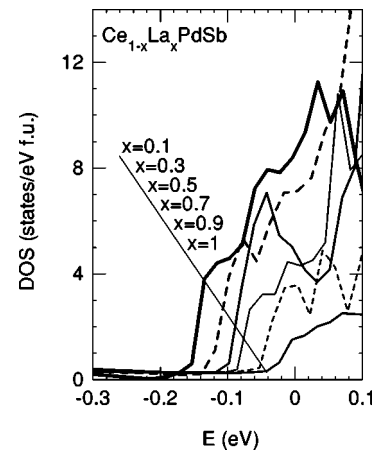

FIG. 3. The total DOS calculated from LMTO for paramagnetic $Ce_{1-x}La_xPdSb$, plotted near the Fermi level.

range of energies in the vicinity of the Fermi energy. CePdSb is calculated by LAPW with the use of LDA XC potential to be half metallic [i.e., $N_\uparrow(\epsilon_F)=7.3$ 1/eVspin, $N_\downarrow(\epsilon_F)=0$], with a magnetic moment of 1.0 μ_B/f.u. roughly consistent with that, reported in Ref. 15 ($\mu_s=0.95$ μ_B), and the electronic specific-heat coefficient γ of 116 mJ/mol-K^2 that is larger
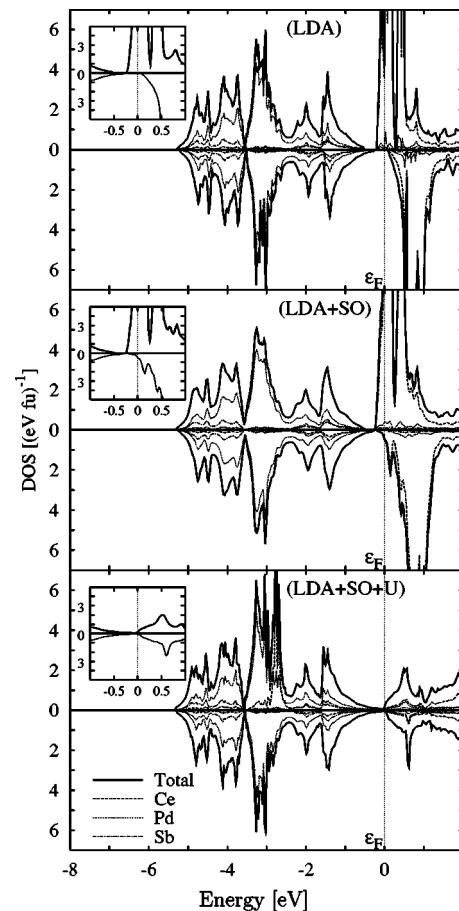

FIG. 4. FP-LAPW calculated total- and atom-spin projected density of states of CePdSb, with the majority plotted upward and minority plotted downward.
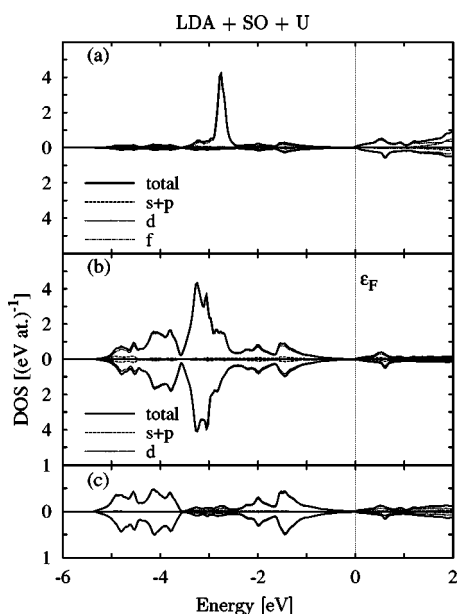
FIG. 5. Atom and symmetry projected FP-LAPW DOS of CePdSb for Ce [in (a)], Pd [in (b)] and Sb [in (c)], respectively.

than the $\gamma = 11$ mJ/mol-K^2 experimentally obtained.[15] The wrong γ-value obtained from this calculation eliminates this method for obtaining the DOS of CePdSb and Ce$_{1-x}$La$_x$PdSb alloys. We, however, present here the results obtained for LDA+XC potential for comparison.

(ii) The LDA+SO method shows the almost half-metallic ground state for CePdSb. The minority DOS obtained at the Fermi energy in the LDA+SO approximation is about 6% of the total DOS at ϵ_F. The calculated magnetic moment per formula unit is 0.95 μ_B.

(iii) The bands obtained with the use of LDA+SO+U correction show the gap for both the spin projections at ϵ_F. The most important result obtained for $U \neq 0$ is the character of the location of the majority 4f Ce states ~2.7 eV below ϵ_F, while the minority 4f DOS is 0 (see Fig. 5). The difference $N_\uparrow(E) - N_\downarrow(E)$ for the f states can be related to ferromagnetism due to more localized than itinerant f states. In this method the magnetic moment localized on the Ce atom is 0.98 μ_B, whereas the total magnetic moment per formula unit (CePdSb) is 1 μ_B. Additionally, the strong Coulomb correlation U separates occupied and empty f states in the spin polarized bands, and in effect, the calculated $\gamma = 3.4$ mJ/mol-K^2 is only $\frac{1}{3}$ of that, obtained experimentally. In case (*iii*) we can interpret the f-electron states as the localized Kondo states [the hybridization between localized f-electron and conduction states can lead to the gap formation (see Fig. 5)], while both situations (*i*) and (*ii*) correspond to the Anderson lattice model and the formation of narrow f band states of width $k_B T_K$, where T_K is a Kondo temperature. It has been controversial whether the Ce ground state in CePdSb is localized or itinerant. The gap Δ_{coh} resulting from LDA+U method should be observed in the resistivity $\rho(T)$ data; this is, however, not the case. Experimental studies for CePdSb[4] and Ce$_{1-x}$La$_x$PdSb compounds do not provide direct evidence of the insulating or semiconducting behavior; the resistivity $\rho(T)$ is not described by an activated law

$\rho = \rho_0 \exp(\Delta_{coh}/k_B T)$ (the resistivity follows an activated behavior, e.g., for Ce$_{1-x}$La$_x$RhSb on the Ce rich side[16]).

Another possibility to answer this question is to compare the XPS VB spectra to the calculated one, obtained with [case (*iii*)] and without [cases (*i*) and (*ii*)] correlation energy U. We, however, did not observe significant differences between all three calculated XPS spectra, especially between 0 and 5 eV, which all are in good agreement to the experimental data. A narrow f electron peak generated by U at ~2.7 eV in the DOS (in Fig. 5) is covered by the Pd d states which dominate the shape of the total DOS, thus its influence on the XPS VB intensities can be neglected. We therefore assume the interference between the ground state calculated in the LDA and LDA+U approximation, respectively. The *mixed ground state* could explain either the experimental γ-value, which is larger than that obtained from LDA+U and smaller than γ calculated from LDA, or the high resistivity value. A local environment of each Ce atom resulting from an atomic disorder could be a reason of the more intricate electronic structure of CePdSb and its alloys. A possible explanation is the formation of two different f DOSs in the electronic band; one, predicted by LDA, and the other one, obtained from LDA+U, which could be attributed respectively to different Ce atoms distributed in the disordered alloy.

The assumption of the *mixed ground state* provides the following simple physical picture. It is assumed that the narrow f band located at ~2.7 eV in the band, interacting via hybridization with a broad Pd d states, delocalizes, which can lead to an enhancement of the DOS at the Fermi level. This process could have a character of fluctuation.

Figure 4 shows the splitting of ~0.3 eV in the projected DOS of the 4f states, which is not well understood. This decomposition of spin-polarized f bands can not be interpreted as the product of the crystal field effect, because the splitting is not reflected in the paramagnetic calculations. We attribute this f band splitting to the Coulomb interaction in the f bands.

The LMTO spin-polarized band calculations performed for the Ce$_{1-x}$La$_x$PdSb series of compounds give evidence (Fig. 6) that the components $x \leq 0.9$ of the series are also half-metals.

B. Ce 3d XPS spectra

Figure 7 shows Ce 3d XPS spectra of Ce$_{1-x}$La$_x$PdSb series, which exhibit different final states depending on the occupation of the f shell: f^1 and f^2 (Refs. 17 and 18). The component, which is a clear evidence of the mixed valence of Ce, was not detected in Ce 3d XPS spectra of CePdSb and its alloys, which suggests a stable configuration of the f shell. The f^2 components located at the low-binding energy side of the f^1 components are attributed within the Gunnarsson–Schönhammer theoretical model to the hybridization between the f states and the conduction band. The hybridization energy $\Delta = \pi V_{fs}^2 N_{max}$ describes the hybridization part of the Anderson impurity Hamiltonian,[19] where N_{max} is the maximum in the DOS and V_{fs} is the hybridization matrix element. Since the intensity ratio $r = I(f^2)/(I(f^1) + I(f^2))$ has been calculated as a function of Δ
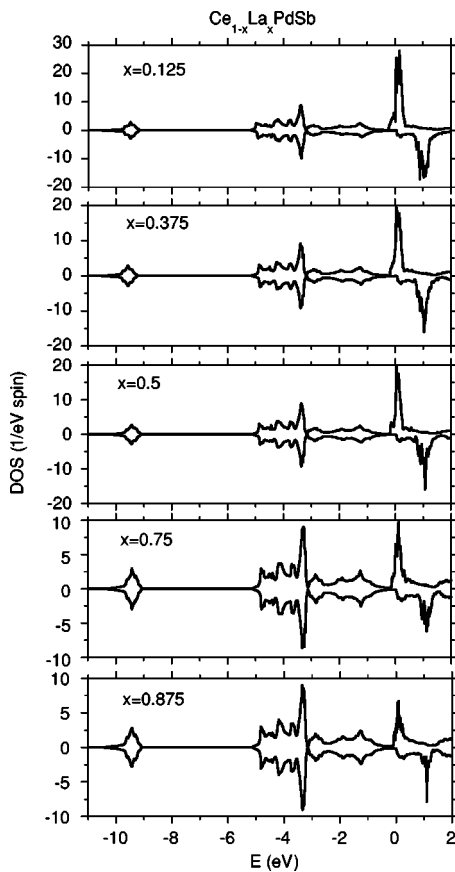
FIG. 6. The LMTO spin-polarized density of states calculated for $Ce_{1-x}La_xPdSb$ series of compounds.

in Ref. 18, it is possible to estimate the hybridization energy Δ, when the peaks of the Ce 3d XPS spectra that overlap in Fig. 7 are separated.[20] The intensity ratio gives for $Ce_{1-x}La_xPdSb$ series a crude estimate of a hybridization width $\sim$80 meV for the components $x \leqslant 0.5$, and $\sim$140 meV for the compounds $x=0.3$ and 0.1. The r and Δ values obtained for different compounds are tabulated in Table II.
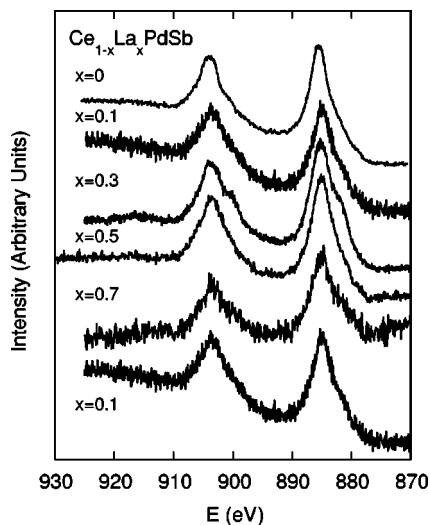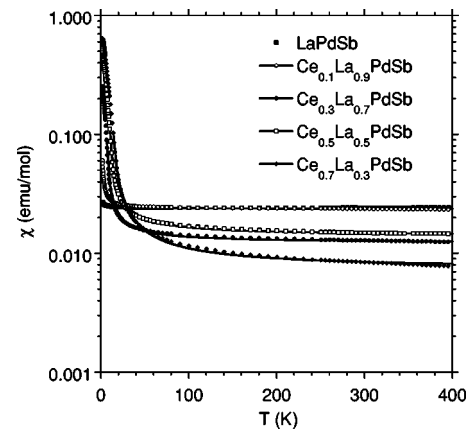

FIG. 7. Ce 3d XPS spectra for $Ce_{1-x}La_xPdSb$.

FIG. 8. Magnetic susceptibility χ measured at $H=0.5$ T versus temperature T for various $Ce_{1-x}La_xPdSb$ samples. The solid line is the Curie–Weiss fit to the data (the parameters for the best fit are tabulated in Table I).

C. Magnetic properties

Shown in Fig. 8 are magnetic susceptibility χ data plotted as χ versus T between 1.9 and 400 K for $Ce_{1-x}La_xPdSb$. The susceptibility above the Curie temperature T_C shows modified Curie–Weiss-type (CW) behavior. Least squares fits of χ to a modified CW law $\chi(T)=\chi_0+C/(T+\theta)$, where $C=N_A\mu_{eff}^2/3k_B$, μ_{eff} is the effective magnetic moment in Bohr magnetons μ_B, and θ is the CW temperature, yield μ_{eff} which decreases with increasing of La concentration in $Ce_{1-x}La_xPdSb$ series (these values are listed in Table I). When the C is renormalized to the number of Ce atoms, all samples (except CePdSb) have nearly the same value of $C \cong 0.46$ emu/mol-K, which gives $\mu_{eff} \cong 1.9$ μ_B/Ce, smaller than that expected for the free ion Ce^{3+}. The values of χ_0 obtained from the fit to the $\chi(T)$ data are smaller in magnitude in comparison to the temperature-independent contribution to the susceptibility in LaPdSb, which is about 2.5×10^{-2} emu/mol (Fig. 8, Table I), suggesting the magnetic contribution to susceptibility of the reference compound LaPdSb.

As can be seen in Fig. 9, the magnetization M curves measured at 1.9 K up to 5 T exhibit similar features in the $Ce_{1-x}La_xPdSb$ compounds. No hysteresis was observed after cycling between $H=\pm5$ T. M achieves saturation above $H=\sim3$ T, providing evidence for ferromagnetism.

As shown in Fig. 10 are electrical resistivity ρ versus T data for $Ce_{1-x}La_xPdSb$ between 4.2 K and 300 K. In order to remove the phonon contribution from $\rho(T)$ of $Ce_{1-x}La_xPdSb$, the $\rho(T)$ data of the isostructural reference compound LaPdSb were subtracted from the $\rho(T)$ data of $Ce_{1-x}La_xPdSb$, under the assumption that the phonon contributions to $\rho(T)$ are similar for both compounds (see inset of Fig. 10).

The resistivity of $Ce_{0.9}La_{0.1}PdSb$, $Ce_{0.5}La_{0.5}PdSb$, and $Ce_{0.1}La_{0.9}PdSb$ is $\sim$450, $\sim$330, and $\sim$300 $\mu\Omega$ cm at $T=300$ K, respectively. These ρ values are very high compared to those observed in several Ce-based compounds (e.g., in Ref. 21). So high resistivity was also observed for CePdSb sample (Ref. 4), the origin of which was not understood. In our view a high resistivity value like these could be

TABLE I. Comparison of structural properties, saturated magnetic moment μ_s, magnetic susceptibility χ and electrical resistivity ρ data for the $Ce_{1-x}La_xPdSb$ samples. The μ_s units and C are per formula unit.

	Lattice parameters		μ_s at $T=1.9$ K	T_C	$\chi=\chi_0+C/(T+\theta)$ (emu/mol)			T_{max}	
x	a (Å)	c (Å)	(μ_B)	(K)	χ_0	C	θ	K	$\rho(T)$ dependence
0	7.913	4.594	0.95	17.5	1.1×10^{-3}	0.59	-11.7; for $T>20$ K		$\rho\propto T^{2.3}$; $T<T_C$ (Ref. 28)
0.1	7.910	4.595		16				215	$\rho\propto T^{2.3}$; $T<T_C$
0.3	7.984	4.596	0.74	12.2	7.3×10^{-3}	0.32	-10.7; for $T>13$ K		
0.5	8.012	4.591	0.50	8.6	14×10^{-3}	0.23	-7.7; for $T>9.5$ K	150	$\rho\propto T^{2.3}$; $T<T_C$
0.7	8.078	4.608	0.32	3.8	12×10^{-3}	0.14	-4.7; for $T>6$ K		
0.9	8.092	4.597	0.14		23×10^{-3}	0.048	-0.6	100	$\rho\propto T^{0.15}$; $T<20$ K
1	8.131	4.606	0.04						

characteristic of the metals with a low carrier concentration.[22]

The samples $x\leqslant0.5$ show the behavior characteristic of magnetic metals. The $\rho(T)$ curves exhibit a pronounced change of slope near the magnetic ordering temperature. The Curie temperature T_C determined as a maximum of $d\rho/dT$ correspond closely to the values obtained from magnetic measurements. The resistivity of ferromagnetic metals at low temperature usually has a magnetic term proportional to T^2, ascribed to one-magnon scattering of conduction electrons (spin-flip scattering).[3] In a HMF all states at the Fermi level are spin polarized, and spin-flip scattering is not possible. Therefore, for a HMF one expects the deviation from a T^2 term in the resistivity (Ref. 2). In our resistivity data for the $Ce_{1-x}La_xPdSb$ samples there is no evidence for such a T^2 contribution at $T<T_C$. The electrical resistivity is $\rho\propto T^\epsilon$ at $T<T_C$, where the power exponents $\epsilon\cong2.3$ in the Ce-rich regime, while for the $Ce_{0.1}La_{0.9}PdSb$ sample $\epsilon\cong0.15$ (Table I).

In the inset of Fig. 10 we display the Ce contribution to the electrical resistivity, $\Delta\rho(T)=\rho(T,Ce_{1-x}La_xPdSb) -\rho(T,LaPdSb)$. The $\Delta\rho$ curve has a maximum at temperature T_{max} (tabulated in Table I), which is a coherence temperature characteristic of the Kondo lattice system. Theoretically, the quantum coherence (i.e., the appearance of heavy quasiparticle states) is associated with the effective Kondo (hybridization) temperature T_K, not with the temperature T_{max} which represents a good characteristic from the experimental point of view. In reality the low-lying excitations in the Anderson- (Kondo-) lattice state appear below $T_K<T_{max}$ which is $T_K=W/2\exp(-1/(J_{fs}N_0))$, where W is the bandwidth with DOS (per atom per spin) at ϵ_F equal to N_0, and J_{fs} is the Schrieffer–Wolf exchange coupling integral,[23] which depends on the location of the $4f$ level in the band and is proportional to $|V_{fs}|^2/\epsilon_{4f}$ in case of $V_{fs}\ll U$. The substitution of La for Ce in $Ce_{1-x}La_xPdSb$ should not distinctly change the local exchange coupling J_{fs}, since $J_{fs}\propto|V_{fs}|^2$ and the hybridization strength is almost x-independent (Table II). [In reality, the substitution of La results in an increase in the unit-cell volume (see Table I). This rise in unit-cell volume leads to a reduction in the Kondo coupling J_{fs}.] On the contrary, $J_{fs}\propto1/\epsilon_{4f}$ depends on the position of the localized $4f$ level with respect to the Fermi level and the intersite Coulomb repulsion U. Thus, when in LDA+SO approximation $\epsilon_F\to0$, J_{fs} increases in magnitude; as result, the magnetic ground state would be expected until J_{fs} becomes so large that the Ce moment is quite quenched.[24] In LDA+U approximation $\epsilon_{4f}\cong2.7$ eV, in result, the Kondo screening is not so high, however, still possible ($\epsilon_{4f}<U$).

What is especially significant is that in the La-rich regime, the electrical resistivity, magnetic susceptibility and the spe-
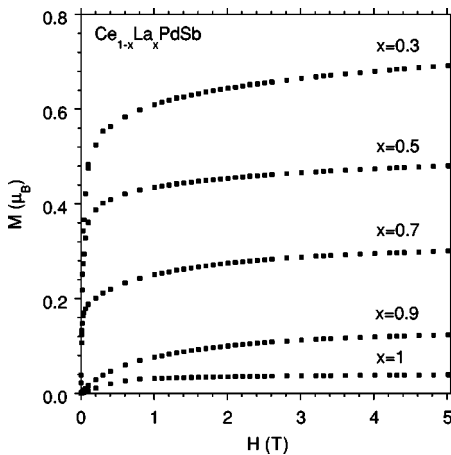

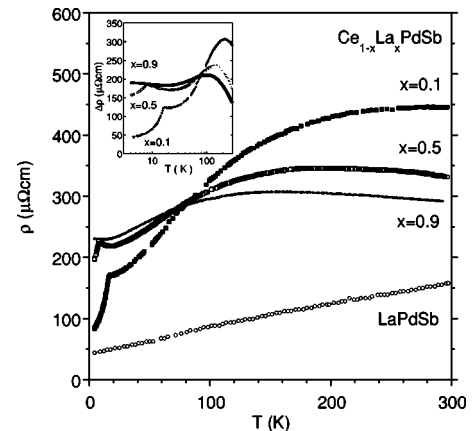FIG. 9. Magnetization M vs. H at $T=1.9$ K for $Ce_{1-x}La_xPdSb$.

FIG. 10. Electrical resistivity ρ vs. T of $Ce_{1-x}La_xPdSb$. Inset shows the resistivity increment $\Delta\rho$ vs. $\ln T$, where $\Delta\rho =\rho(Ce_{1-x}La_xPdSb)-\rho(LaPdSb)$.

TABLE II. The intensity ratio $r=I(f^2)/(I(f^1)+I(f^2))$ obtained for the both spin-orbit components $3d_{5/2}$ and $3d_{3/2}$ of the Ce 3_d XPS spectra, and the hybridization energy Δ.

$Ce_{1-x}La_xPdSb$	r	Δ (in meV)
$x=0$	0.14	~ 60
$x=0.1$	0.15	~ 70
$x=0.3$	0.2	~ 100
$x=0.5$	0.16	~ 80
$x=0.7$	0.24	~ 110
$x=0.9$	0.29	~ 140

cific heat exhibit power laws characteristic of non-Fermi liquid (NFL) behavior. Shown in Fig. 11 are $\Delta\rho$ and $\Delta C/T$ versus $\ln T$ and $\Delta\chi$ versus T on a double logarithmic scale for $Ce_{0.1}La_{0.9}PdSb$. The Ce contributions to $\rho(T)$, $\chi(T)$, and $C(T)/T$ in $Ce_{0.1}La_{0.9}PdSb$ have the following T dependences:

(i) $\Delta\rho(T)=\Delta\rho(0)[1-a(T/T_K)^\epsilon]$, with $\epsilon \approx 0.15$, $T_K=4$ K, and $a=0.14$. The T dependence of the resistivity increment $\Delta\rho(T)$ could be determined by subtracting the lattice contribution of LaPdSb. Thus, to exclude the possibility that subtraction of the background contribution to $\rho(T)$ could generate the NFL exponent seen in the incremental resistivity $\Delta\rho(T)$ we have compared the power-law exponents for the as-measured resistivity obtained between 4.2 and 16 K. The power-law exponent ϵ is exactly the same (Table I).

(ii) $\Delta\chi(T)=c(T/T_K)^{-1.4}$ for $T<20$ K. The best fit to the

experimental data gives $T_K=4$ K and $c\equiv\chi(0)=0.08$. The susceptibility exponent is close to the $\frac{3}{2}$ expected for mean-field model of a Kondo alloy with randomly distributed magnetic impurities.[25]

(iii) Between 2.7 and 7 K, $\Delta C(T)/T$ can be fitted to either a $-\ln T$ or $b(T/T_K)^{-1.6}$ dependence, where $b\equiv\gamma(0)=98$ mJ/molK^2, and $T_K=5$ K, thus, the Kondo disorder model is also a candidate for NFL-type behavior. It is amazing that the NFL characteristics are observed for the Ce-diluted system, suggesting a magnetic critical point at $0.1<x<0.3$ region. Experiments on a variety of f-electron systems (e.g., $Y_{1-x}U_xPd_3$, Ref. 26) suggest, however, that the NFL behavior can be observed in contiguity to the region in which spin glass freezing occurs, i.e., for $x=0.2$. The scaling of $\Delta\rho(T)$, $\Delta C(T)$ or $\Delta\chi(T)$ with T_K suggests that NFL-like behavior is a single ion phenomenon that is associated with the Kondo effect.

We would like to comment on a value of $T_K\cong 4$ K obtained for $Ce_{0.1}La_{0.9}PdSb$ from various experiments, which is much less than $T_{max}\cong 100$ K, at which the electrical resistivity has a broad maximum. Treating the system as a dilute alloy, Cornut and Coqblin (Ref. 27) suggested that the broad maximum in resistivity, such as that observed in CePdSb and $Ce_{1-x}La_xPdSb$, is associated with the combined effect of the crystalline electric fields (CEFs) on the $4f$ moments and Kondo-type interaction. This theory predicts different Kondo temperatures corresponding to different crystal-field levels. The experimental results in Fig. 10 support this prediction; the first $\Delta\rho\sim\ln T$ dependence corresponds to the Kondo effect on the total $(J=\frac{5}{2})$ manifold, and a second one for $T\ll\delta_{CEF}$ corresponds to the Kondo effect on the ground state level(s).
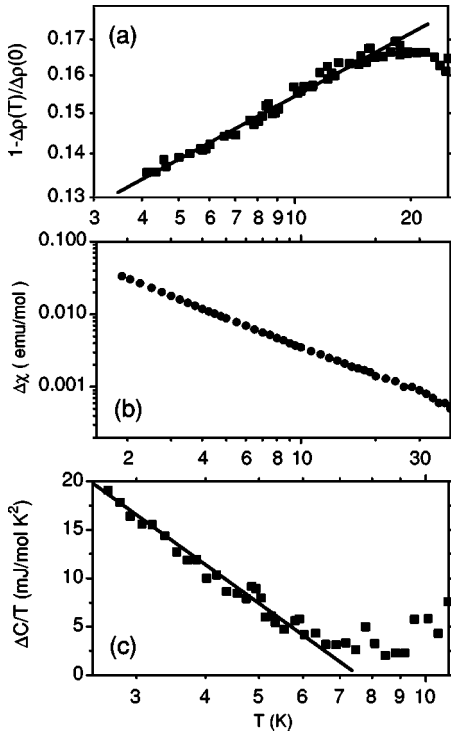

FIG. 11. $Ce_{0.1}La_{0.9}PdSb$: (a) $1-\Delta\rho(T)/\Delta\rho(0)$ vs. $\ln T$; (b) $\Delta\chi$ vs. T in a double logarithmic scale, where $\Delta\chi=\chi(Ce_{0.1}La_{0.9}PdSb)-\chi(LaPdSb)$; and (c) specific heat $\Delta C/T$ vs. $\ln T$, where $\Delta C=C(Ce_{0.1}La_{0.9}PbSb)-C(LaPdSb)$.

D. Concluding remarks

We have shown that the numerical calculations of the electronic density of states leads to the HMF properties of CePdSb. An energy gap for the minority band structure was determined by LMTO and FP-LAPW (LDA, LDA+SO) methods, which give the magnetic moment of CePdSb very close to the saturation magnetization obtained experimentally from M versus H dependence at $T=1.9$ K.

It has been, however, controversial whether the ground state of CePdSb is in the HMF or on metallic state. Electrical resistivity of CePdSb is very large[4] and $\rho(T)\propto T^\epsilon$, where $\epsilon>2$ in the temperature range $T<T_C$, indicative of the HMF state, whereas the Hall coefficient $R_H(T)$ is strongly anisotropic[28] and it shows a T-scaling for $H\|c$, $I\|a$, characteristic of ferromagnetic metals,[29] i.e., $R_H\propto\alpha T^3+\beta T^4$ for $T<T_C$, and unusual low-temperature behavior for $H\|a$, $I\|c$ below T_C. In addition, experimental data in Ref. 28 reported the low carrier concentration of about $0.011/f.u.$ for CePdSb, expected for HMF.

We are well aware that these experimental results only indirectly motivate the HMF properties of CePdSb and $Ce_{1-x}La_xPdSb$ alloys. In other words, the HMF state in these compounds is rather hypothetical from the experimental point of view, whereas band structure calculations predict the

HMF properties explicitly. Specifically, spin polarized photoemission studies are necessary.

We have shown that the LDA and LDA+SO approximations predict the HMF character of the CePdSb, while the LDA+U potential predicts much more localized f-electron states which are located in the majority band ~ 2.7 eV below ϵ_F, and the gap at ϵ_F for both spin directions. This result is, however, in contradiction to the resistivity $\rho(T)$ experimental observation, which has not shown an activated behavior.

The half-metallic ground state was also calculated for the $Ce_{1-x}La_xPdSb$ compounds, which are for $x \leq 0.7$ ferromagnetic. The ferromagnetic Kondo-lattice state transforms gradually into the NFL state in the regime $x > 0.7$. The sample with $x = 0.9$ shows a non-Fermi liquid behavior, and the power-law exponents of $\Delta\chi$, $\Delta\rho$, and $\Delta C/T$ are expected by the Kondo-disorder model. $Ce_{0.1}La_{0.9}PdSb$ is a rare example of the Ce-diluted alloy which exhibits a NFL-like behavior attributed to the one (majority) spin projection.

[1] R. A. de Groot, F. M. Mueller, P. G. van Engen, and K. H. J. Buschow, Phys. Rev. Lett. **50**, 2024 (1983).

[2] M. J. Otto, R. A. M. van Woerden, P. J. van der Valk, J. Wijngaard, C. F. van Bruggen, and C. Haas, J. Phys.: Condens. Matter **1**, 2351 (1989).

[3] I. Mannari, Prog. Theor. Phys. **22**, 335 (1959).

[4] S. K. Malik and D. T. Adroja, Phys. Rev. B **43**, 6295 (1991).

[5] Y. Baer, G. Busch, and P. Cohn, Rev. Sci. Instrum. **46**, 466 (1975).

[6] O. K. Andersen and O. Jepsen, Phys. Rev. Lett. **53**, 2572 (1984); O. K. Andersen, O. Jepsen, and M. Sob, in *Electronic Structure and Its Applications*, edited by M. Yussouff (Springer, Berlin, 1987), p. 2.

[7] U. von Barth and L. Hedin, J. Phys. C **5**, 1629 (1972).

[8] C. D. Hu and D. C. Langreth, Phys. Scr. **32**, 391 (1985).

[9] P. Blaha, K. Schwarz, G. K. H. Madsen, D. Kvasnicka, and J. Luitz, *WIEN2k, An Augmented Plane Wave + Local Orbitals Program for Calculating Crystal Properties* (Karlheinz Schwarz, Techn. Universitat Wien, Austria, 2001), ISBN 3-9501031-1-2.

[10] J. P. Perdew, K. Burke, and M. Ernzerhof, Phys. Rev. Lett. **77**, 3865 (1996).

[11] V. I. Anisimov, J. Zaanen, and O. K. Andersen, Phys. Rev. B **44**, 943 (1991); V. I. Anisimov, F. Aryasetiawan, and A. I. Lichtenstein, J. Phys.: Condens. Matter **9**, 767 (1997).

[12] A. I. Lichtenstein, V. P. Antropov, and B. N. Harmon, Phys. Rev. B **49**, 10 770 (1994).

[13] J. J. Yeh and I. Lindau, At. Data Nucl. Data Tables **32**, 1 (1985).

[14] S. Tougaard and P. Sigmund, Phys. Rev. B **25**, 4452 (1982).

[15] O. Trovarelli, J. G. Sereni, G. Schmerber, and J. P. Kappler, Phys. Rev. B **49**, 15 179 (1994).

[16] S. K. Malik, L. Menon, K. Ghosh, and S. Ramakrishnan, Phys. Rev. B **51**, 399 (1995).

[17] O. Gunnarsson and K. Schönhammer, Phys. Rev. B **28**, 4315 (1983).

[18] J. C. Fuggle, F. U. Hillebrecht, Z. Zolnierek, R. Lässer, Ch. Freiburg, O. Gunnarsson, and K. Schönhammer, Phys. Rev. B **27**, 7330 (1983).

[19] P. W. Anderson, Phys. Rev. **124**, 41 (1961).

[20] S. Doniach and M. Šunjić, J. Phys. C **3**, 286 (1970).

[21] D. Wohlleben and B. Wittershagen, Adv. Phys. **34**, 403 (1985).

[22] M. J. Otto, H. Feil, R. A. M. van Woerden, J. Wijngaard, P. J. van der Valk, C. F. van Bruggen, and C. Haas, J. Magn. Magn. Mater. **70**, 33 (1987).

[23] J. R. Schrieffer and P. A. Wolff, Phys. Rev. **149**, 491 (1966).

[24] S. Doniach, Physica B & C **91**, 231 (1977).

[25] D. R. Grempel and M. J. Rozenberg, Phys. Rev. B **60**, 4702 (1999).

[26] B. Andraka and A. M. Tsvelik, Phys. Rev. Lett. **67**, 2886 (1991).

[27] B. Cornut and B. Coqblin, Phys. Rev. B **5**, 4541 (1972).

[28] K. Katoch, T. Takabatake, A. Ochiai, A. Uesawa, and T. Suzuki, Physica B **230–232**, 159 (1997).

[29] Yu. P. Irkhin, A. N. Voloshinskii, and Sh. Sh. Abelskii, Phys. Status Solidi **22**, 309 (1967).